Geochimica et Cosmochimica Acta 400 (2025) 115–128

Contents lists available at ScienceDirect

Geochimica et Cosmochimica Acta

journal homepage: www.elsevier.com/locate/gca

Systematics of helium diffusion sinks in apatite demonstrated by $^4He/^3He$ degassing experiments and modeling

Hongcheng Guo [a,*], Marissa M. Tremblay [a], Peter K. Zeitler [b], Bruce D. Idleman [b], Annia K. Fayon [c]

[a] Department of Earth, Atmospheric, and Planetary Sciences, Purdue University, West Lafayette, IN 47906, United States
[b] Department of Earth and Environmental Sciences, Lehigh University, Bethlehem, PA 18015, United States
[c] Department of Earth Sciences, University of Minnesota, Minneapolis, MN 55455, United States

ARTICLE INFO

Associate editor: Cecile E Gautheron

Keywords:
Apatite
Thermochronology
Diffusion
(U-Th)/He
$^4He/^3He$

ABSTRACT

Widely reported overdispersion of apatite (U-Th)/He ages has encouraged efforts to explore He diffusion kinetics and systematics in apatite. Studies such as continuous ramped heating (CRH) of apatite have revealed complex laboratory He behavior that is often correlated with abnormally old (U-Th)/He ages. Stemming from these studies is a hypothesis that diffusion sinks within apatite grains can reversibly trap radiogenic ^4He over both geologic time and during laboratory heating. This sink-related trapping is further hypothesized to be temperature dependent and can hence potentially provide thermal-history information. In this work, we conducted $^4He/^3He$ degassing experiments from proton-irradiated apatite samples using a CRH-like heating strategy. We demonstrate that the synthesized ^3He also exhibits complex release behavior which (1) confirms that the proposed sink-related trapping occurs during laboratory heating, and (2) provides foundational evidence for possibly qualifying the nature and quantifying the abundance and/or distribution of diffusion sinks. Our combined $^4He/^3He$ observations show that an apatite sample's thermal history controls the amount of trapping over geologic time. Building upon the dataset from one of the sink-bearing samples, we attempt to simulate the sink characteristics using a simple random-walk code that can simulate trapping. The forward modeling can reproduce the ^3He release observed in the laboratory experiment if multiple sinks characterized by different kinetics are present. Using such sink kinetics and the sample's known thermal history, we find that the prediction of laboratory ^4He release, which reflects both geologic and laboratory volume diffusion and trapping processes, is comparable to our observations. This work confirms that a temperature-dependent trapping mechanism is required to explain the complex He diffusion behavior seen in many apatite grains, and also serves as a proof-of-concept that helium trapped in sinks can provide added thermal history information.

1. Introduction

Apatite (U-Th)/He and $^4He/^3He$ thermochronometry (hereafter AHe thermochronometry) have become widely used tools in studies of tectonic, surficial, and other geologic processes at various timescales (e.g., Drake and Reiners, 2021; Gautheron and Zeitler, 2020; McDannell et al., 2022; Min et al., 2003; Reiners et al., 2005; Tremblay et al., 2015). Development of the AHe method has co-occurred with these applications owing to an increasing demand for understanding of the diffusion systematics of He in apatite (e.g., Djimbi et al., 2015; Farley, 2000; Gerin et al., 2017; Shuster et al., 2006; Shuster and Farley, 2004, 2009; Wolf et al., 1996; Zeitler et al., 1987). This growing body of work has led to the frequent observation of overdispersion in AHe ages that is beyond what analytical uncertainty and current helium diffusion models allow. A range of factors can complicate the ^4He systematics in apatite in ways that makes it difficult to interpret apparent ages, such as U and Th zonation (Fitzgerald et al., 2006; Meesters and Dunai, 2002), the presence of U-rich inclusions (Farley, 2002), broken grains (Beucher et al., 2013; Brown et al., 2013), and ^4He implantation (Murray et al., 2014; Spiegel et al., 2009). Study of this overdispersion has also allowed recognition of grain-specific variations in the diffusion systematics of ^4He in apatite, most noticeably encouraging the development of radiation-damage models (Flowers et al., 2009; Gautheron et al., 2009; Willett et al., 2017). These radiation damage models have become the

* Corresponding author.
E-mail address: guo750@purdue.edu (H. Guo).

https://doi.org/10.1016/j.gca.2025.05.036
Received 29 January 2025; Accepted 23 May 2025
Available online 25 May 2025

dominant means of interpreting overdispersed ages and attempts to gain additional time–temperature information from them. However, in more than a few cases, particularly from older, more slowly cooled settings, (U-Th)/He datasets exhibit dispersion in excess of what radiation damage, grain size (e.g., Reiners and Farley, 2001), and other aforementioned factors can explain, and it has been broadly recognized by the low-temperature thermochronology community that more fundamental work needs to be done to better understand the complexities of He diffusion behavior (Ketcham et al., 2022; Zeitler et al., 2017a).

The advance of using continuous ramped heating for laboratory analysis (CRH; Idleman et al., 2018) enabled a critical observation: the diffusion, or more broadly speaking the mobilization, of He in apatite is controlled by mechanisms beyond volume diffusion, which is a fundamental assumption of both simple diffusion models (e.g., Wolf et al. 1996) and models in which radiation-damage accumulation and annealing (Flowers et al., 2009; Gautheron et al., 2009; Willett et al., 2017) have been taken into account (Guo et al., 2021; McDannell et al., 2018). In a CRH analysis, a single grain of apatite is heated continuously with a linear temperature ramp, and outgassing ^{4}He is simultaneously accumulated and measured. The CRH analysis reveals the release patterns of ^{4}He and offers some information about diffusion kinetics and systematics. Idleman et al. (2018) demonstrated that ^{4}He release by volume diffusion should result in unimodal incremental degassing curves that have been frequently observed in Durango apatite fragments (Fig. 1A). However, the ^{4}He release patterns are sometimes found to be more complex (Fig. 1B). Complex release patterns can be characterized by ^{4}He released as sharp spikes and/or, most notably, as a secondary release of ^{4}He at significantly higher temperatures than what volume diffusion theory predicts, often in the form of a discrete gas-release peak and sometimes in the form of a broader band (i.e., gas release that spans a range of temperatures without forming discrete peaks).

Guo et al. (2021) found that such complex release patterns are correlated with overdispersed and anomalously old AHe ages and invoked the suggestion by Zeitler et al. (2017b) that some apatite grains can possess crystal imperfections that act as diffusion sinks, trapping radiogenic ^{4}He as it is transported by volume diffusion. Mobilization of helium out of a sink can be parameterized with a finite escape energy and a temperature-dependent escape probability (Zeitler et al., 2021). The sink is also thought to be thermally stable during laboratory helium degassing, as demonstrated by cycled heating experiments by Guo et al. (2024a). We also suspect that the sink is a separate type of crystal imperfections from radiation damage, or at least from our current understanding of radiation damage and its effect on helium behavior (Flowers et al., 2009; Gautheron et al., 2009; Willett et al., 2017) as all nature apatites contain radiation damage but not all suffer from complex helium release. In the development of the concept of sink, a critical addition in the model proposed by Guo et al. (2021) is that in analyzed grains, trapping takes place twice, first during the apatite grain's geologic thermal history and later during laboratory heating. In this hypothesis, the high-temperature (i.e., "anomalous") release of ^{4}He represents radiogenic ^{4}He that was trapped in diffusion sinks over geologic time as well as any ^{4}He that was trapped in the sinks during laboratory heating. The laboratory trapping is controlled by the kinetics of the sinks as well as the laboratory heating schedule, which is a known parameter. The geologic trapping, on the other hand, is impacted by both the sinks' kinetics and the sample's thermal history. The slower that a sample cools through temperatures at which partial ^{4}He retention will occur, the higher the probability that ^{4}He diffusing by random walking will be trapped into the sinks, simply because there is more radiogenic production across an interval during which ^{4}He is mobile. Therefore, samples that cool slowly during their geologic history can exhibit much older AHe ages in the presence of diffusion sinks, whereas samples quenched at a high cooling rate should see little or no geologic trapping and therefore little to no increase in age.

The influence of diffusion sinks should also apply to thermal histories inferred from apatite ^{4}He/^{3}He thermochronometry. Apatite ^{4}He/^{3}He thermochronometry (Shuster and Farley, 2004) utilizes the intracrystalline ^{4}He and ^{3}He distribution to quantify an apatite grain's geologic thermal history at low temperatures. In this method, ^{3}He is produced by spallation reactions during proton irradiation (Shuster and Farley, 2004). The proton irradiation is designed such that a spatially uniform and high concentration of ^{3}He is produced within individual irradiated mineral grains. The distribution of radiogenic ^{4}He, on the other hand, is non-uniform and is dictated mainly by the thermal history of a sample as well as any zoning in U and Th. The evolution of the ^{4}He/^{3}He ratio during stepwise degassing of a proton-irradiated apatite grain is therefore directly related the spatial distribution of the radiogenic ^{4}He. In apatite grains for which existing models of radiation damage-controlled volume diffusion is sufficient to explain helium mobilization, we can utilize the measured ^{4}He/^{3}He evolution, conventional (whole-grain) (U-Th)/He date, and a helium diffusion model to model an apatite grain's thermal history. Thermal histories modeled with apatite ^{4}He/^{3}He data are better constrained than models with conventional (U-Th)/He dates alone and can provide information on cooling down to temperatures as low as 30–40 °C.

The hypothesis that apatite can contain helium diffusion sinks raises several critical questions about the (U-Th)/He system that can be addressed with apatite ^{4}He/^{3}He thermochronometry. Each question represents a knowledge gap that cannot be answered with CRH measurements alone, and together they represent a potential opportunity to

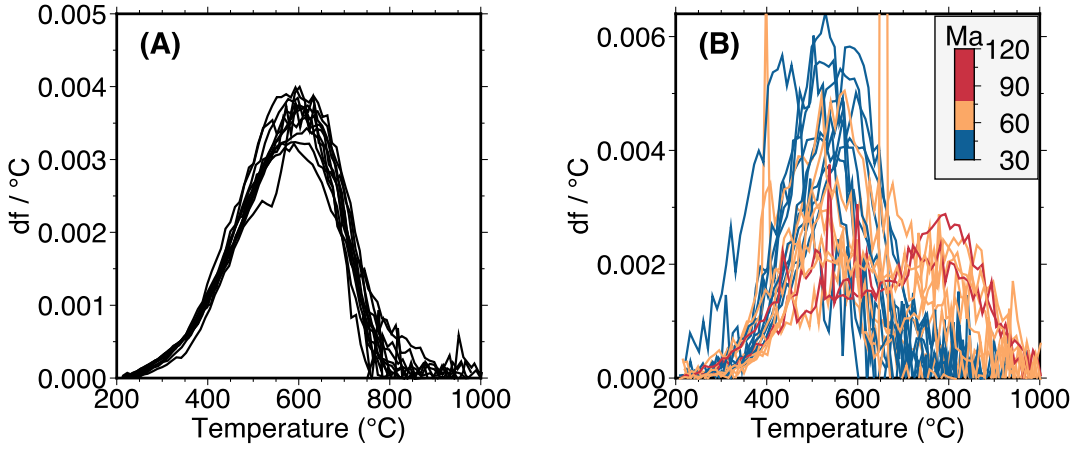

Fig. 1. Examples of ^{4}He release patterns from CRH analysis. **(A)** Simple unimodal release behavior observed from Durango apatite fragments. **(B)** Simple and complex release behaviors observed from Transantarctic Mountains (TAM) apatite grains. Individual grain analyses are colored according to their (U-Th)/He age. Revised after Guo et al. (2024a).

move AHe thermochronometry forward.

(1) Does complex laboratory degassing behavior also occur for ^{3}He?

The observations of radiogenic ^{4}He made by previous CRH analyses cannot directly differentiate geologic and laboratory trapping. Proton-induced ^{3}He, on the other hand, has no 'geologic memory' and is spatially uniform at the single crystal scale before laboratory heating. We would expect that proton-induced ^{3}He, like ^{4}He, will show diffusion behavior consistent with trapping into diffusion sinks during laboratory degassing.

(2) Does laboratory ^{3}He release provide information about trapping kinetics of diffusion sinks in apatite, such that the observed laboratory ^{4}He/^{3}He release in the presence of sinks offers additional thermal history information?

If the answer to *question (1)* is yes, an important subsequent question is whether ^{3}He release can provide information about the trapping kinetics of diffusion sinks in apatite in the context of ^{4}He/^{3}He thermochronometry. Crucially, however, the amount of trapping for ^{3}He should be less than that for ^{4}He, and should provide a direct constraint on trapping behavior, given the known heating schedule and the uniform ^{3}He starting condition. If we can recover information about the trapping kinetics of diffusion sinks in an apatite grain from the proton-induced ^{3}He, we will have grain-specific helium diffusion kinetics that can be incorporated into thermal history models that predict the observed ^{4}He/^{3}He release spectrum. This may provide greater constraints on the thermal histories permissible given an observed ^{4}He/^{3}He release spectrum, or it may enable us to model the thermal histories of complex release spectra that cannot be reconciled with existing volume diffusion models.

To address the above questions, we first performed a series of laboratory step-heating ^{4}He/^{3}He experiments on apatite grains from samples that have distinct thermal histories. Based on previous work, apatite grains in some of these samples can show complex CRH spectra consistent with the presence of diffusion sinks (Guo et al., 2021, 2024a). We evaluated step-heating results using three kinds of data presentation: (1) the step-wise percentage of ^{4}He and ^{3}He released as a function of temperature, which allows for a direct examination of overall diffusion behavior and allows us to answer *question (1)*; (2) the ratio of ^{4}He/^{3}He released from each heating step relative to the bulk ^{4}He/^{3}He ratio, plotted as a function of cumulative ^{3}He release, which allows for a closer look at how a sample's thermal history impacts the proposed trapping, and (3) Arrhenius plots showing the apparent diffusivities of ^{3}He and ^{4}He as a function of temperature, which can be used to make inferences about the influence of diffusion sinks on helium diffusion kinetics, thereby shedding light on *question (2)*.

Next, we used a forward model that simulates a random-walk diffusion process in the presence of reversible sinks to further address *question (2)*. This modeling was designed to infer the volume diffusion and trapping kinetics of sinks that predict the observed laboratory ^{3}He release. We then used such diffusion and trapping kinetics to simulate geologic ^{4}He retention and laboratory release using the known thermal history information of the samples, evaluating the potential of using diffusion-sink trapping kinetics to recover additional information about the samples' thermal histories. We also compare the ^{4}He simulations from alternative thermal histories to test the sensitivity of the modeled trapping kinetics of diffusion sinks.

2. Methods

2.1. Materials

Our diffusion experiment uses well-characterized apatite samples from Durango, Mexico, the Transantarctic Mountains (TAM), and the German Continental Deep Drilling holes (KTB). All three of these sample suites have been dated and studied via CRH analysis (Guo et al., 2021, 2024a; Idleman et al., 2018) as well as conventional AHe measurements (Fitzgerald et al., 2006; Guo et al., 2024a; McDannell et al., 2018; Warnock et al., 1997). Each of these apatite samples (Table 1) has specific qualities that suit our experiment design in order to answer our overarching questions. First, we analyzed internal fragments from a *gem*-quality crystal of Durango apatite from the Cerro de Mercado mine near Durango City, Mexico (Young et al., 1969). Durango apatite formed in a quench-cooled geological setting and is known for its reproducible (U-Th)/He age of 31.44 ± 0.18 Ma (2σ) (Gautheron et al., 2021; McDowell et al., 2005), serving as an age standard in the AHe community. Durango apatite has an atypically high effective uranium concentration ([eU] = U + 0.238Th + 0.0012Sm; Cooperdock et al. (2019)) ranging from ~ 40 to greater than 100 ppm, an unusual Th/U ratio of ~ 20 (Boyce and Hodges, 2005), and can exhibit significant U and Th zoning (Boyce and Hodges, 2005). However, to date the Durango apatite fragments analyzed by CRH have exhibited exclusively simple ^{4}He degassing behavior (~20 fragments) as predicted by volume-diffusion theory (Guo et al., 2024a; Idleman et al., 2018; McDannell et al., 2018). Durango apatite has also shown simple ^{4}He degassing behavior in published conventional step-heating analyses (e.g., Farley, 2000; Shuster and Farley, 2004; Wolf et al., 1996). Therefore, in this study Durango serves as a reference for ^{4}He and ^{3}He diffusion behavior. What is also critical for the ^{4}He/^{3}He analysis conducted in this study is that analyzing internal fragments ensures an initial spatially uniform distribution of both radiogenic ^{4}He and synthetic ^{3}He. For Durango fragments, there should be neither a thermally controlled, geological diffusion profile nor alpha-ejection profiles of ^{4}He, and ^{3}He should have no prior concentration profile at all.

Second, we analyzed TAM single-grain apatite crystals (sample R22646 from Cathedral Rocks, Fitzgerald et al., 2006). These apatite crystals have been thoroughly studied for AHe dating and for their ^{4}He degassing behavior (e.g., Fitzgerald et al., 2006; Guo et al., 2021). TAM samples are known for their dispersed AHe ages and frequently complex ^{4}He degassing patterns that are inconsistent with simple radiation-damage-controlled volume-diffusion behavior (Guo et al., 2021). What is most important for this work is that Fitzgerald et al. (2006) found that TAM apatite crystals experienced slow, generally monotonic cooling

Table 1
Sample information and (U-Th)/He ages.

Sample	Source	Multi-grain Reference Age by Guo et al. (2021, 2024a)	Observed Age This Study
Dur1	Durango, Mexico (Young et al., 1969)	~28–35 Ma (n = 15)	34.43 ± 0.46 Ma
Dur2			30.34 ± 1.23 Ma
TAM1	TAM, original sample R22646 (Fitzgerald et al., 2006)	Mostly ~ 30–80 Ma (n = 18) with some ~ 140–340 Ma (n = 2)	48.87 ± 1.21 Ma
TAM2			287.85 ± 5.32 Ma
KTB-3502	KTB Borehole, original sample KTB-3502 (Warnock et al., 1997)	~2–77 Ma (n = 8)	7.82 ± 0.15 Ma
KTB-2954	KTB Borehole, original sample KTB-2954 (Warnock et al., 1997)	~20–137 Ma (n = 9)	58.39 ± 2.42 Ma
KTB-920–1	KTB Borehole, original sample KTB-920 (Warnock et al., 1997)	~32–70 Ma (n = 6)	77.17 ± 2.48 Ma
KTB-920–2	KTB Borehole, original sample KTB-920 (Warnock et al., 1997)		80.02 ± 2.03 Ma

through the He partial retention zone (PRZ) at rates of ~ 1°C/Myr from the Cretaceous to the early Cenozoic and ~ 2.8 °C/Myr since then via apatite fission track thermochronometry.

Third, we analyzed KTB single apatite crystals (sample KTB-920, KTB-2954, and KTB-3502, Warnock et al., 1997) that were sourced from a borehole at depths of 920 m, 2954 m, and 3502 m. The sample KTB-920 cooled through the He PRZ at a rate of ~ 2 °C/Myr and has an equilibrium temperature of ~ 27 °C (Wolfe and Stockli, 2010). The samples KTB-2954 and KTB-3502 have equilibrium temperatures of ~ 87 °C and ~ 103 °C, respectively (Wolfe and Stockli, 2010). The two deeper samples experienced a distinctive thermal history relevant to this study: for many millions of years, the apatite grains from each sample remained at or above temperatures necessary to behave as a completely open system in conventional apatite helium diffusion models.

Apatite grains or fragments from these samples were irradiated with protons at the Francis H. Burr Proton Therapy Center at the Massachusetts General Hospital in March 2022 within a ~ 555 mm-long target. The target was irradiated with protons of 229 MeV energy for ~ 9 h with an intensity of ~ 10^{11} protons/cm^2/s. The total proton fluence was 9.98 x 10^{15} protons/cm^2, and the target was rotated 180° halfway through the irradiation to ensure it received a symmetrical axial exposure to protons. There has been no statistically significant difference in the diffusion kinetics determined via measurements of radiogenic ^{4}He and proton-induced ^{3}He (Shuster and Farley, 2004, 2005). In addition, the damage associated with proton irradiation is mostly electronic, which is different from that from neutron irradiation, which is more akin to radiation damage (Shuster and Farley, 2009). Therefore, we anticipate that the irradiation would not hinder the potential of observing complex helium release behavior from the samples. Optically clear fragments (in the case of Durango) or unbroken individual grains (in case of all other samples) were selected with a stereomicroscope to avoid visible inclusions and internal cracks. The selected grains and fragments were photographed and their dimensions measured. We analyzed two Durango standards and multiple TAM and KTB single grains with ^{4}He/^{3}He step-heating experiments, with the goal of observing TAM and KTB grains that exhibited complex degassing behavior.

2.2. ^{4}He/^{3}He step-heating experiments

Individual selected apatite grains or fragments were placed in a niobium (Nb) tube with the ends of the Nb tube crimped closed and with the junction of a K-type bare wire thermocouple inserted in one end. We then loaded the Nb tube into a larger platinum-iridium (PtIr) tube. The wires of the thermocouple were entwined and welded to the posts of a K-type ultra-high vacuum thermocouple feedthrough that was mounted into an ultra-high vacuum laser microfurnace with a sapphire viewport and connected to an ultra-high vacuum extraction line. Sample heating was accomplished using a 910 nm, 130 W diode laser defocused over the PtIr package, with temperature regulated via a closed-loop controller to ± 2 to 5 °C of the target setpoint. After each heating step, the gas was first cleaned by two SAES GP 50-ST 101 getters, one operated at ambient temperature and one operated at ~ 250 °C, then cryogenically focused using a Janis CCS-TRAP-HT/204 closed-cycle cold trap, and finally measured with an Isotopx NGX Helium Plus sector field mass spectrometer. The NGX Helium Plus at Purdue is outfitted with a high sensitivity cathode 'Nier' type gas source and five detectors: two Faraday cups with ATONA® amplifiers, and three discrete dynode electron multipliers. For all step-heating experiments the ^{4}He amount was small enough that all helium isotope measurements could be performed on an electron multiplier. At the beginning of each measurement, we peak centered using the composite HD peak, which has a constant background intensity in the NGX between ~ 150 and 250 cps. We then measured ^{4}He and ^{3}He signal intensities by peak hopping, with 15 cycles and 15 measurements per cycle for each isotope. The extraction line and mass spectrometer were pumped for at least 20 min between each heating step.

We made blank corrections by measuring 'cold' extraction line blanks, both with the diffusion cell and the standard pipette volumes. Cold diffusion cell and pipette volume blanks are not distinguishable from 'hot' blanks measured by heating empty packets (analyzed separately from these experiments). We determined the mass spectrometer sensitivity by measuring the helium isotopic composition of a manometrically-calibrated gas standard that was created by mixing pure ^{4}He and ^{3}He, with a ^{3}He/^{4}He of 0.00238. We can measure four different size aliquots of this standard gas: one using the 0.2020 ± 0.0002 cm^3 pipette volume in front of the standard tank, and three by expanding an aliquot in the pipette into two ~ 3 cm^3 calibrated safety volumes in front of the pipette. We do not observe a significant dependence of instrument sensitivity on ^{4}He signal intensity (a proxy for pressure, e.g., Burnard and Farley, 2000) over the range of standard aliquots analyzed, and all heating measurements had ^{4}He signal intensities within the range of standard intensities. We analyzed an extraction line blank and gas standard pipettes at the beginning of each experiment as well as between every 4–6 heating steps.

The heating schedules that we used in our ^{4}He/^{3}He step-heating experiments were designed as a hybrid of conventional ^{4}He/^{3}He step-heating analysis (e.g., Shuster and Farley, 2004; Tremblay et al, 2015) and CRH analysis (e.g., Guo et al., 2021; Idleman et al., 2018). This work did not used actual CRH-style ^{4}He/^{3}He analysis, which would be performed with a continuous linear heating ramp and simultaneous gas accumulation and measurement, because (1) the number of ^{3}He atoms is not large enough for accurate determination of fractional loss data during a continuous measurement, and (2) there is significant potential risk involved in exposure of a magnetic sector mass spectrometer to an actively heated sample chamber. Our experiments are like traditional step-heating experiments in that multiple heating steps are involved with pumping between the steps. Conventional step-heating experiments, however, target well-proportioned if not evenly distributed gas release at each step to avoid small beams having greater relative uncertainties. Because we were interested in the finer details of gas release during analysis, our heating schedule was closer to a "low resolution" version of CRH: each heating step has the same duration of one hour, and temperatures were raised by an equal amount for each subsequent prograde heating step. Most of our experiments started from 186 °C, and each following step was hotter by ~ 24 °C. This type of "linear" ramping of temperature facilitates data presentation and assessment and enables us to distinguish unimodal distributions of step-wise gas release, much like a CRH experiment. One of the exceptions to this was the experiment on sample 'Durango1', for which we used a heating schedule that is slightly different from a linear one. Another exception was the experiment on sample 'KTB-2954', for which the heating schedule was linear but involved shorter durations per heating step but a larger number of total steps. Heating schedules and helium isotope data are reported in the Research Data section.

Following ^{4}He/^{3}He experiments, the degassed grains or fragments were dissolved, and the parent U-Th-Sm isotopes were measured by isotope dilution at the University of Illinois Urbana-Champaign Helium Analysis Lab (HAL) using a Thermo Scientific iCAP^{TM} quadrupole inductively coupled plasma mass spectrometer, following the procedures reported in Guenthner et al (2016). The apatite samples in this study have (U-Th)/He ages consistent with previously reported results (Table 1).

2.3. DIFFSIM: simulation of helium diffusion in sink-presented crystals

For comparison with our step-heating experiments we performed forward simulations of helium diffusion in the presence of sinks in order to explore how different thermal histories as well as diffusion-sink kinetics could influence ^{4}He and ^{3}He gas release. We used a version of the DIFFSIM code (github.com/OpenThermochronology/diffsim), which simulates diffusion as a series of independent 3D random walks for helium atoms over both geologic timescales and laboratory heating (Zeitler

et al., 2021). This code is described in more detail in the online repository, but we provide a brief overview here.

In DIFFSIM, the diffusion random walk is simplified as occurring along three orthogonal axes with equal probability and with no interactions between the helium atoms, simulating isotropic volume diffusion in a crystal lattice with a spherical geometry and allowable occupancy sites for He atoms that are equally spaced along the x, y, and z axes of a Cartesian grid. Walkers are created at random positions, and the code incorporates alpha ejection. Provided the number of grid nodes is sufficient (~10^6 or more) and sufficient walkers are used (~10^5 to 10^6 atoms), the code perfectly simulates the bulk diffusion process as described by analytical solutions. In the frequency factor, diffusivity and grain size trade off with one another. Thus, by arbitrarily setting the grid size such that each diffusion jump is size 1 cm, it is easy to scale diffusivity to give a frequency factor that simulates diffusion in apatite, using the Einstein expression for diffusivity as a function of jump distance and jump frequency. A small number of nodes in the modeled crystal grid are randomly declared to be diffusion "sinks" into which He can become reversibly trapped. The probability p of escaping from a diffusion sink during a time interval dt is an empirical exponential function of temperature T and an escape energy E_{trap}. This distribution is normalized to produce a maximum probability of 1 at the specified scale temperature T_{scale}. The time interval dt adjusts the probability to be relevant to time steps in both the geologic and laboratory-heating phases of the model.

$$p = dt exp^{\frac{-Etrap}{RT}} / exp^{\frac{-Etrap}{RTscale}} \quad (1)$$

where R is the gas constant and all other variables are as defined above. Combinations of the sink escape activation energy and scale temperature can be chosen to simulate the temperature range across which escape can occur. Note that while empirical, this probability expression captures the temperature dependence of higher-temperature (i.e., "anomalous") helium release seen in many samples. DIFFSIM allows the presence of multiple sink types having different trapping parameters. Walkers trapped in sinks are offered one chance for escape per time step, scaled by probability, and those that escape return to the normal volume-diffusion walk; note that it is possible for an atom to be trapped and escape multiple times.

This simulation framework has a few simplifying assumptions. First, the simulation does not accurately simulate apatite crystallography. For the purposes of the model (investigating how diffusion and trapping might interact) and given the need to maintain reasonable execution speeds, this is not a major issue since diffusivity is scaled to observed values. Next, the simulation does not currently take into account the accumulation and annealing of radiation damage, which are known to occur in natural apatite and influence He diffusion kinetics (Flowers et al., 2009). However, the TAM and KTB samples used in this work do not have high concentrations of effective uranium (eU): eU ranges from 5.2 to 41.2 ppm for the analyzed grains with the exception of sample KTB-3502, which has an eU of 152.1 ppm (See Data Repository.) Therefore, the effect of radiation damage for these samples would be at most a second-order control on helium diffusivity and age dispersion (Guo et al., 2021, 2024a). Third, the sinks in this simulation are designed as static features, meaning that they do not evolve and/or anneal during a sample's geologic history or laboratory heating during the simulation. In reality, they might evolve as a function of temperature, although previous CRH experiments suggest that, at least in the laboratory degassing, the sinks are thermally persistent (Guo et al., 2024a). Again, given the goals of the code and its success in simulating observed first-order features of helium release, it would be premature to complicate the model as the nature of the imperfections that act as sinks and their behavior are an area of active research.

We simulated apatite containing sinks in varying numbers and escape activation energy to produce laboratory ^{3}He release similar to the observations made from one of our step-heating samples, TAM2. The simulation consists of a geologic history followed by laboratory heating, the latter of which uses the same heating schedule as that we used in our step-heating experiments, ultimately predicting ^{4}He release as a function of temperature. The ^{3}He data are predicted by simulating an isothermal, no-diffusion geologic history with no alpha-ejection profile to produce the proton-induced uniform distribution of ^{3}He. The volume diffusion process is simulated with sample-specific volume diffusion kinetic parameters obtained from the measured ^{3}He release data. These kinetic parameters were obtained by regressing a line through all consecutive low temperature Arrhenius data (i.e., heating steps before "anomalous" high-temperature gas releases) that give highest R^2, which in our case is always greater than 0.99. Using these sample-specific volume diffusion kinetic parameters, and combining sink amounts and types (300–2000 sink locations and sink escape activation energy of 25–80 KCal/mol), we simulated the ^{4}He releases using the known geologic thermal history of the TAM2 sample as well as other alternative thermal histories. We compared the simulated ^{4}He releases to our laboratory observations to evaluate whether the addition of sinks in the diffusion model make a first-order impact on trapping ^{4}He in the way conceptualized by our hypothesis. We also evaluated how sensitive the sink trapping is to various thermal histories. In the Supplementary Material, we included additional DIFFSIM simulation results using various parameters for sinks (Fig. S2) and thermal histories (Fig. S3) to more fully demonstrate how DIFFSIM predictions respond to different inputs.

3. Results

Durango apatite fragments should show unimodal gas release in response to progressive heating, as found by CRH analysis of ^{4}He (Guo et al., 2021; Idleman et al., 2018). Such fragments should also yield a constant ratio of ^{4}He to ^{3}He for all heating steps during ^{4}He/^{3}He analysis. The two Durango internal fragments we analyzed showed similar gas release (Fig. 2A, D) below ~ 550 °C. Sample Dur1 exhibits unimodal release of both ^{4}He and ^{3}He (Fig. 2A). Because the analyzed internal fragments have no geologic diffusion profile, the ratio of ^{4}He and ^{3}He released from each heating steps (R_{step}) generally equals the ratio of total ^{4}He and ^{3}He released (R_{bulk}), and the R_{step}/R_{bulk} data are equal to 1 within analytical uncertainty (Fig. 2B). In comparison, sample Dur2 shows a small secondary high-temperature gas release (Fig. 2D) but the R_{step}/R_{bulk} for Dur2 is still ~ 1 (Fig. 2E). For both samples, Arrhenius data for ^{4}He and ^{3}He are not significantly different throughout the experimental temperature range. Arrhenius trends, except for the high temperature part of sample Dur2, are comparable to conventional step-heating result of Durango apatites obtained by Farley (2000) (Fig. 2 C, F).

TAM apatite grains are expected to show a wide range of gas-release behaviors, as found by previous studies using CRH (Guo et al., 2021; Idleman et al., 2018; McDannell et al., 2018). In the absence of complex behavior, the R_{step}/R_{bulk} data from TAM samples should plot within the R_{step}/R_{bulk} zone permitted by diffusion and alpha ejection (Fig. 5 in Shuster and Farley, 2004), and the R_{step}/R_{bulk} data should show a gradual increase with cumulative ^{3}He released, consistent with relatively slow cooling through the He PRZ. Sample TAM1 has a unimodal gas release for both ^{4}He and ^{3}He (Fig. 3A), and the R_{step}/R_{bulk} data fall into the plausible R_{step}/R_{bulk} zone, except for the last data points which comprise < 1 % of the total gas (Fig. 3B). The Arrhenius trends for both ^{4}He and ^{3}He in TAM1 are similar to that of the Durango reference line from Farley (2000) with comparable slopes (activation energy) but lower y-intercept (pre-exponential factor). There is no obvious difference in the apparent kinetics between the ^{4}He and ^{3}He data (Fig. 3C) beyond systematically lower $\ln(D/a^2)$ of ^{4}He that is known to result from diffusive rounding near the grain rim, and the high-temperature data points converge together. In contrast, sample TAM2 shows two release peaks for both ^{4}He and ^{3}He, including a ^{4}He-only release spike (Fig. 3D; spikes are defined as one or a few heating steps that break the monotonic increasing or decreasing of the gas loss trend, and the step-wise gas loss

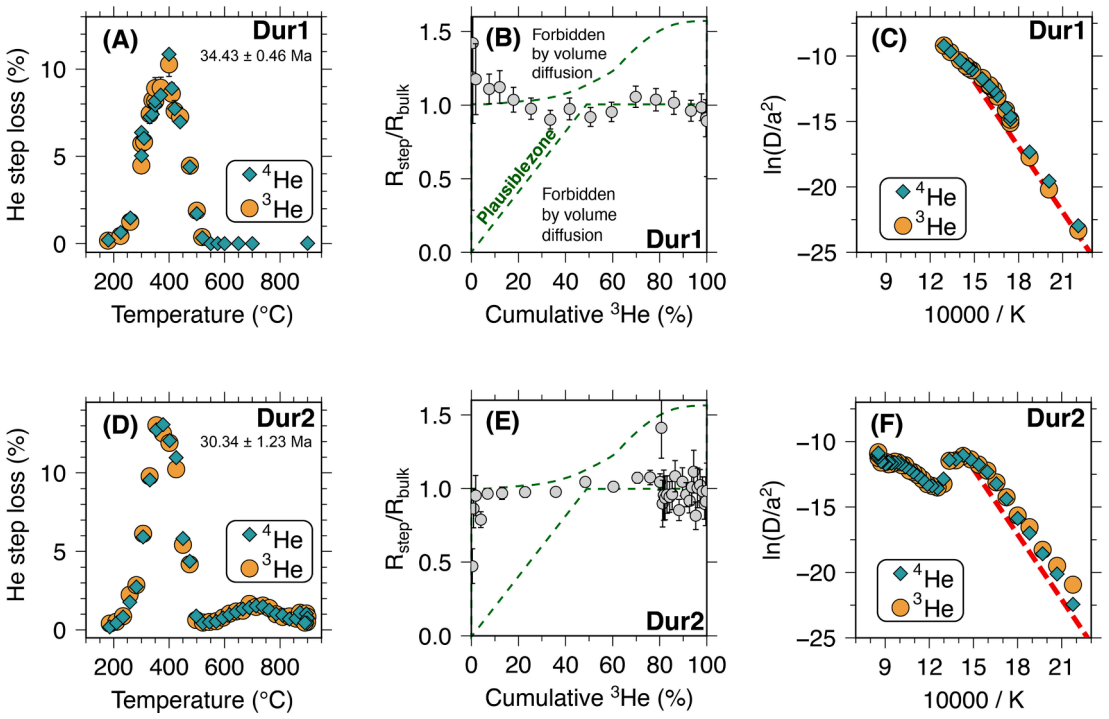

Fig. 2. Step-heating results for Durango samples. (A, D) ^{4}He and ^{3}He fractional release data. The percent of gas released from each heating step is plotted versus temperature. AHe ages are given for each sample beneath the sample name. (B, E) ^{4}He and ^{3}He ratio profiles. Ratio of ^{4}He and ^{3}He released from each heating step (R_{step}) is normalized by the ratio of total ^{4}He and ^{3}He released (R_{bulk}). These normalized ^{4}He/^{3}He ratios are plotted versus cumulative ^{3}He release (%). Plausible zone . (C, F) Arrhenius plots with reference red dashed line from Farley (2000).

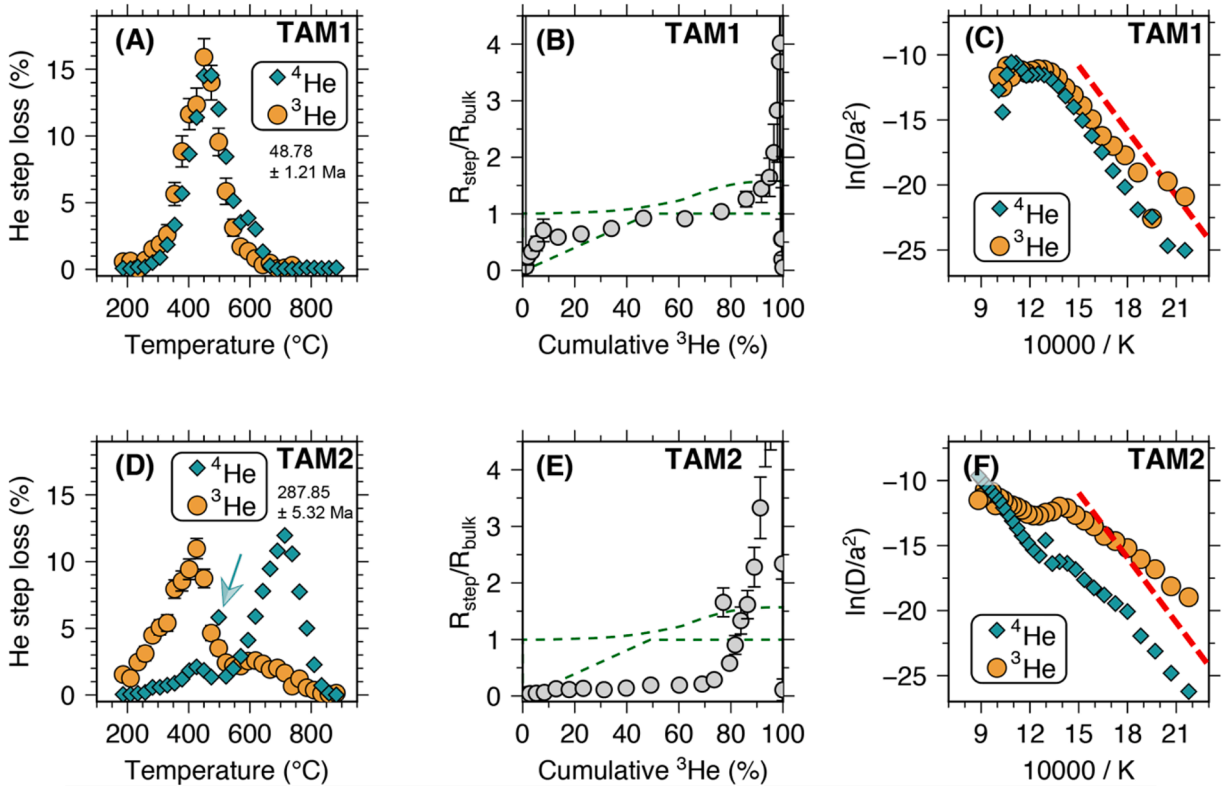

Fig. 3. Step-heating results for TAM samples. (A, D) ^{4}He and ^{3}He fractional release data. AHe ages are given for each sample. Arrows indicate gas spikes. (B, E) ^{4}He and ^{3}He ratio profiles. Ratios greater than 4 are not shown. (D, F) Arrhenius plot with reference red dashed line from Farley (2000).

is higher than the neighboring heating steps by at least 2 % of total gas.). The ^{4}He step-wise loss at higher temperature heating steps (i.e., ~500–900 °C) constitutes a larger proportion of the total ^{4}He, as compared to ^{3}He for which the high-temperature release constitutes smaller fraction of total ^{3}He (Fig. 3D). Many R_{step}/R_{bulk} data points fall outside of the plausible R_{step}/R_{bulk} zone (Fig. 3E). For the first ~ 80 % of total ^{3}He release, the R_{step}/R_{bulk} values are much lower than expected, and for the last > ~10 % of total ^{3}He release, the R_{step}/R_{bulk} values are much higher than expected. The low-temperature Arrhenius trends for ^{4}He and ^{3}He in TAM 2 show a significant difference in diffusivities while maintaining similar slopes (Fig. 3F). Additionally, the low-temperature Arrhenius trends suggest a lower activation energy and pre-exponential factor than that of the reference line from Farley (2000).

KTB apatite grains are expected to generate either simple unimodal or complex release behavior for the shallow sample KTB-920 and to show either complex release behavior or little gas retention for the two deep samples, KTB-3502 and KTB-2954, as revealed by previous CRH work (Guo et al., 2024a). Two grains from sample KTB-920 yielded exclusively simple degassing results (Fig. S1 in Supplementary Material). Here, we focus on our results from other KTB samples: two apatite grains from depths of 3502 and 2954 m, respectively, that are in or below the PRZ for conventional He diffusion in apatite, both show unique and complex degassing behavior (Fig. 4A, D). For both grains, the release of ^{4}He does not start in earnest until ~ 380 °C, and the majority of the gas is released at higher temperatures. However, as a comparison during the earliest heating steps, ^{3}He release (circles, Fig. 4A, D) has already begun for both samples. For KTB-3502, ^{4}He (diamonds, Fig. 4A) is released mostly at higher temperatures, except fora spiky data point at ~ 450 °C. The ^{3}He release also clearly persists to temperatures greater than 800 °C, although the low- and high-temperature release are not well separated as discrete release peaks. KTB-2954 yield similar result, except that both ^{4}He and ^{3}He show spikes at ~ 400–420 °C. Similar to that of the sample TAM2, many R_{step}/R_{bulk} data points from the KTB samples fall outside of the plausible R_{step}/R_{bulk} zone (Fig. 4B, E). The Arrhenius trend of ^{3}He for KTB-3502 suggests a gradual change of the kinetics from being comparable to those for the Durango reference line at low temperatures toward higher retentivities at higher temperatures (Fig. 4C), with the slope (activation energy) eventually returning to the value observed at the lower temperatures. The gradual change is compatible with the observation that there is no discrete ^{3}He peak at high temperatures (Fig. 4A). The Arrhenius array of ^{4}He for this sample largely sits below the reference line from Farley (2000) owing to very little ^{4}He release at low temperatures. We obtained similar results from KTB-3502, except that the significant spike in the ^{4}He release results in large break in the Arrhenius array (Fig. 4F).

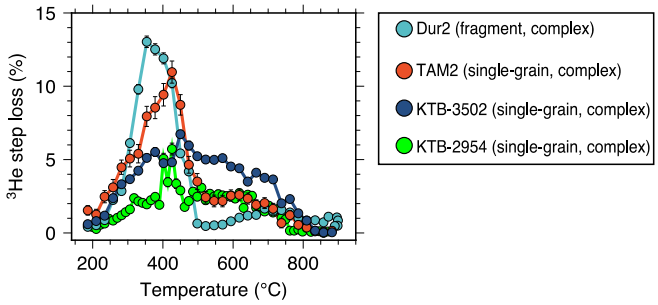

Fig. 5. Comparison of ^{3}He release data from samples that have complex gas-release behavior.

4. Discussion

4.1. *^{3}He shows trapping behavior in apatite*

The trapping of ^{3}He during our step-degassing experiments demonstrates that helium trapping can occur during laboratory heating. The

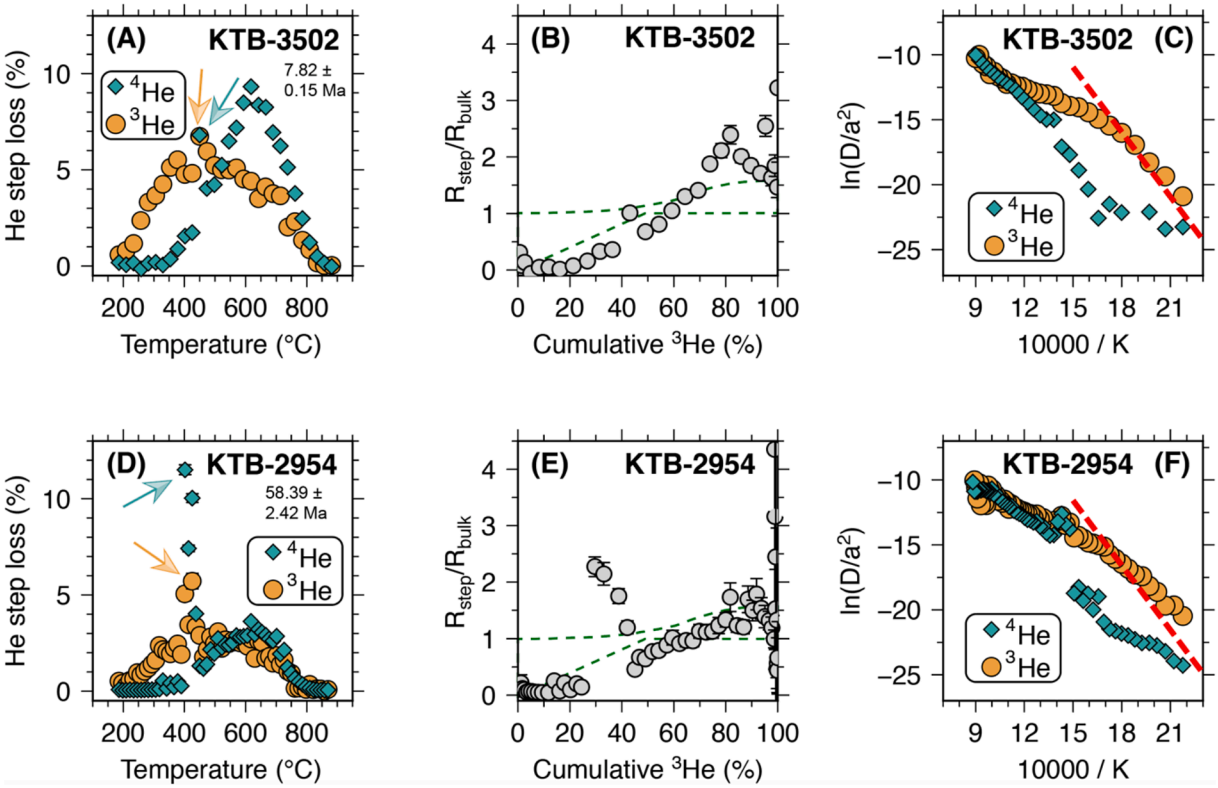

Fig. 4. Step-heating results for KTB samples. (A) (D) ^{4}He and ^{3}He fractional release data. AHe ages are given for each sample beneath the sample name. Arrows indicate gas spikes. (B) (E) ^{4}He and ^{3}He ratio profiles. Ratios greater than 4 are not shown. (D) (F) Arrhenius plot with reference red dashed line from Farley (2000).

combined observation of low ^{4}He solubility in apatite (Zeitler et al., 2017b) and the high-temperature ^{4}He-release identified from CRH (Guo et al., 2021; McDannell et al., 2018) has led to the diffusion sink hypothesis (Guo et al., 2021; McDannell et al., 2018; Zeitler et al., 2017b, 2021), in which diffusing helium, once it has entered a void-like sink, will have difficulty returning to the lattice. Although this trapping model has been tested and shown to have a kinetic nature (Guo et al., 2024a), an important question remains: does the sink-related ^{4}He have to be extraneous (i.e., analogous to excess argon in ^{40}Ar/^{39}Ar thermochronometry) or can it be internally produced (McDannell et al., 2018)? Earlier CRH work was able to infer that trapped components do not have to be extraneous and likely represent internally generated radiogenic ^{4}He trapped over geologic time (Guo et al., 2021, 2024a).

In the current study, because the ^{3}He was initially uniformly distributed in the apatite samples with no geologic trapping before the step-heating experiments, we can confirm that the laboratory heating process itself induces trapping of helium, transporting lattice-accommodated helium to sink localities. Therefore, ^{4}He need not be extraneous to produce the high-temperature release observations made by CRH analyses or the experiments presented here. This observation verifies the suggestions that internally generated radiogenic ^{4}He will be trapped both over geologic time and during laboratory heating. The observation also offers insights on what crystal imperfections might act as sinks in apatite. If the helium associated with sinks were of extraneous origin, we would suspect the sinks to be linked to fluid or mineral inclusions. Our findings suggest that apatite grains do not necessarily have to possess such inclusions to exhibit sink-related helium trapping.

4.2. Diffusion sinks vary from grain to grain

Previous work using CRH analysis demonstrated that apatite grains from the same rock sample with the same geologic thermal history can yield differing patterns of high-temperature ^{4}He release, hinting at the occurrence of variability in the abundance and/or kinetics of helium diffusion sinks (Guo et al., 2021; McDannell et al., 2018). In this work, our observations of ^{3}He release provide direct visualization of the variation of laboratory sink-trapping, since the ^{3}He release behavior is not impacted by the sample's geologic history. For the four experiments exhibiting complex helium release behavior (Dur2, TAM2, KTB-3502, and KTB-2954), a comparison of the ^{3}He release fraction as a function of temperature (Fig. 5) suggests that the proportion of ^{3}He released as part of the first release peak (or broadly speaking at lower temperatures in the case of sample KTB) versus that at the second release peak (or at higher temperatures) differs from sample to sample. Above 500 °C, the ^{3}He released can account for as little as 20 % but as much as 50 % of total ^{3}He released from a grain. The shapes of these high-temperature release pattern are also clearly different from grain to grain, implying that the kinetics characterizing diffusion sinks likely also vary from grain to grain, or that multiple sink types are present. We explore these potential kinetic differences in the following modeling section.

Another lesson we learn from our ^{4}He/^{3}He experiments concerns the nature of gas spikes observed during the step heating (e.g., Fig. 3D; Fig. 4A, D). Such spikes have been reported in CRH work (Guo et al., 2021, 2024a; McDannell et al., 2018). McDannell et al. (2018) suggested that gas spikes could be related to decrepitation of fluid inclusions. The presence of a ^{3}He spike seems to rule out this possibility for the case of co-occurring ^{4}He and ^{3}He spikes. Guo et al. (2024a) speculated that the spikes could be related to diffusion sinks that happen to be near crystal surfaces and are therefore more prone to physical disruption, releasing a large fraction of gas upon doing so. Our ^{4}He/^{3}He experiments support this possibility, because (1) we have now also observed gas spikes of ^{3}He as well and (2) the ^{3}He in spikes is generally less abundant relative to the ^{4}He than we would otherwise predict (e.g., Fig. 4A, D). This is shown by the sudden increase of the R_{step}/R_{bulk} values across some spikes. Because ^{3}He experiences sink-related trapping only in the lab, it is reasonable to expect a deficit of ^{3}He relative to ^{4}He associated with spikes, since ^{4}He also has a geologically trapped component. However, ^{3}He does not always co-occur with ^{4}He in spikes. For example, sample TAM2 shows only a ^{4}He spike but no associated ^{3}He spike (Fig. 3D); this might suggest that gas spikes can result from crystal imperfections of different types, and in this case the aforementioned decrepitation of U-bearing inclusions is a viable explanation.

4.3. Implications of sink-trapping for retrieving Arrhenius data

In considering our results, we realize that the kinetics data calculated by conventional means for samples with complex release behavior may violate some assumptions. For example, a convention in noble gas thermochronology has been to use the total gas released as a reference for calculating fractional losses per heating step (e.g., Fechtig and Kalbitzer, 1966). However, in the case of apatite samples that yield significant high-temperature release due to hypothesized trapping in diffusion sinks, inclusion of the high-temperature component in the total loss causes a significant underestimation of the true loss values for the early release presumed to be related to "normal" volume diffusion. This effect is nonlinear, and even a modest high-temperature release does not change results significantly, but as the size ratio between low- and high-temperature components approaches 1 or greater, apparent diffusivities

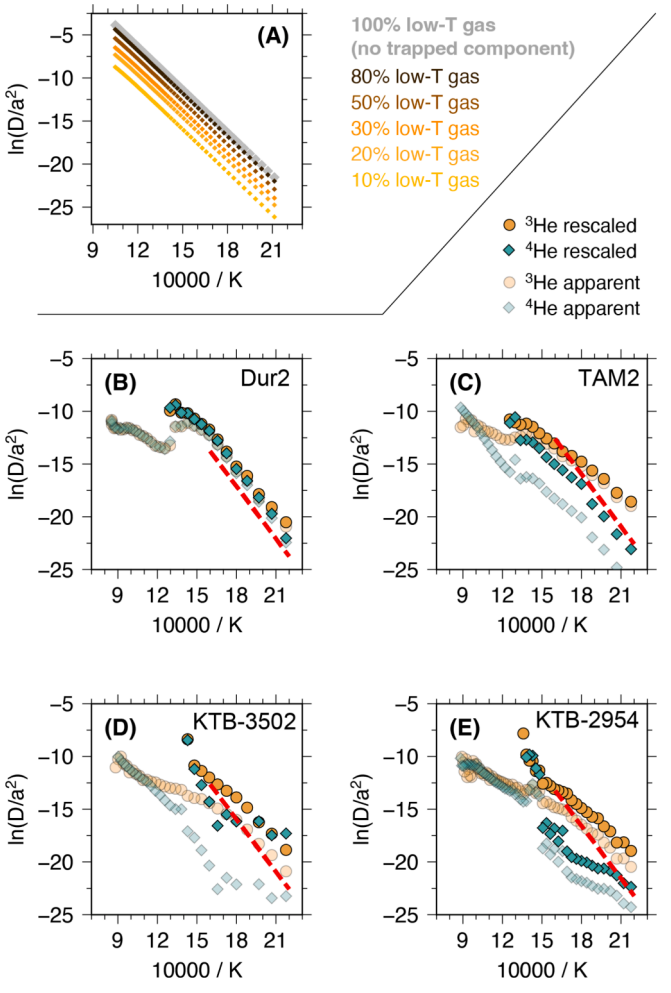

Fig. 6. **(A)** Simulation showing the decrease in apparent diffusivities expected as the fraction of low-temperature gas release that is unaffected by trapping in diffusion sinks decreases. The decrease becomes significant as the fraction of gas released at low temperatures represents less than 50% of total. Diffusivities of sample Dur2 **(B)**, TAM2 **(C)**, KTB-3502 **(D)**, and KTB-2954 **(E)**, rescaled using the helium abundance measured at the end of the low-temperature phase of gas release.

calculated using the conventional methodology drop significantly. Fig. 6A shows an example, calculated for a Durango-like sample with of D_0 50 cm^2/s and E_a of 33 Kcal/mol (138 KJ/mol), that demonstrates how apparent diffusivities decrease with progressive underestimation of fractional losses due to the trapped gas component.

In attempt to account for this assumption, we rescaled the observed fractional losses of helium for samples that display complex gas release using measured He abundance at the end of the low-temperature phase of gas release as the total release value for kinetics calculations. The dividing temperature for low-temperature versus high-temperature is roughly adapted from the gas release plots (Fig. 2D; 3D; 4A, D) to be the point where a local minimum in stepwise helium loss is observed (often at ~ 450–500 ℃, but variable based on sample size, kinetics, heating schedule, etc.). We found that the diffusivities recalculated using this method generally sit close to or above the Durango reference lines (Farley, 2000). Note that the exception shown in Fig. 6E, with low $\ln(D/a^2)$ for ^{4}He, which is caused by the sizable amount of ^{4}He released as a gas spike that occurs before the dividing temperature and which therefore effectively leads to under-calculation of the fractional losses. Overall, this recalculation of kinetics parameters in an attempt to remove the effects of trapping leads to greater similarity in apparent kinetics behavior between samples and closer agreement with reference results from samples not significantly affected by trapping (Farley, 2000).

4.4. Geologic thermal-history information recorded by diffusion sinks

A consequential question that arises from our ^{4}He/^{3}He experiments is whether trapping by diffusion sinks is sensitive to the details of a sample's thermal history. If so, it might be possible to obtain additional thermal-history information from grains containing sinks if the kinetics and systematics of trapping can be determined.

Our experiments support this idea. Sample Dur2, which does show some trapping, experienced a quenched volcanic thermal history. In this scenario, our diffusion-sink model would predict little ^{4}He accumulation in sinks thanks to very small amounts of diffusive random walking of ^{4}He across geologic time (Fig. 7A, B).Therefore, the high-temperature release has to be only from laboratory heating. This is verified by the nearly identical ^{4}He and ^{3}He release, suggesting that all trapping of ^{4}He occurred during laboratory heating (Fig. 2C). In contrast, sample TAM2 spent a considerable time at temperatures near the partial retention zone (PRZ) for helium in apatite, leading to a greater chance of trapping for more radiogenic ^{4}He during cooling (Fig. 7A, C). This is observed in the high-temperature gas releases in that the high-temperature component of ^{4}He comprises a large proportion of total gas compared to that ^{3}He (Fig. 3D). Finally, samples KTB-3502 and KTB-2954 represent extreme endmembers for our models, as they have been residing at temperatures just above the conventional apatite-helium PRZ for an extended time, and they should have little or no conventional ^{4}He retention. Any ^{4}He accumulated in these grains should therefore be trapped in sinks (Fig. 7A, D). Our observations again match this prediction, as little ^{4}He was released across the earlier heating steps, while significant ^{3}He release occurred during these early steps. Most of the ^{4}He was released during high-temperature heating steps.

The impact of thermal history on trapping manifests not just in the release patterns of ^{4}He and ^{3}He, but also in the R_{step}/R_{bulk} data. For samples showing trapping, these ratios fall outside the zone that is possible assuming only alpha ejection and sink-free volume diffusion: we observed lower-than-expected normalized ratios from low-temperature heating steps and higher-than-expected normalized ratios from high-temperature heating steps (Fig. 3B, E and 4B, E). An immediate outcome of these results is that, using an appropriate heating schedule, laboratories that can perform ^{4}He/^{3}He analysis can diagnose significant trapping in their measured samples without careful temperature regulation during laser step heating, or without having to set up a dedicated system for CRH analysis.

However, a more ambitious outcome emerges: is it possible to obtain additional thermal-history information from apatite samples containing sinks? We explore this question using DIFFSIM simulations of our TAM2 dataset. We chose this sample for several reasons. First, Dur2 is not an

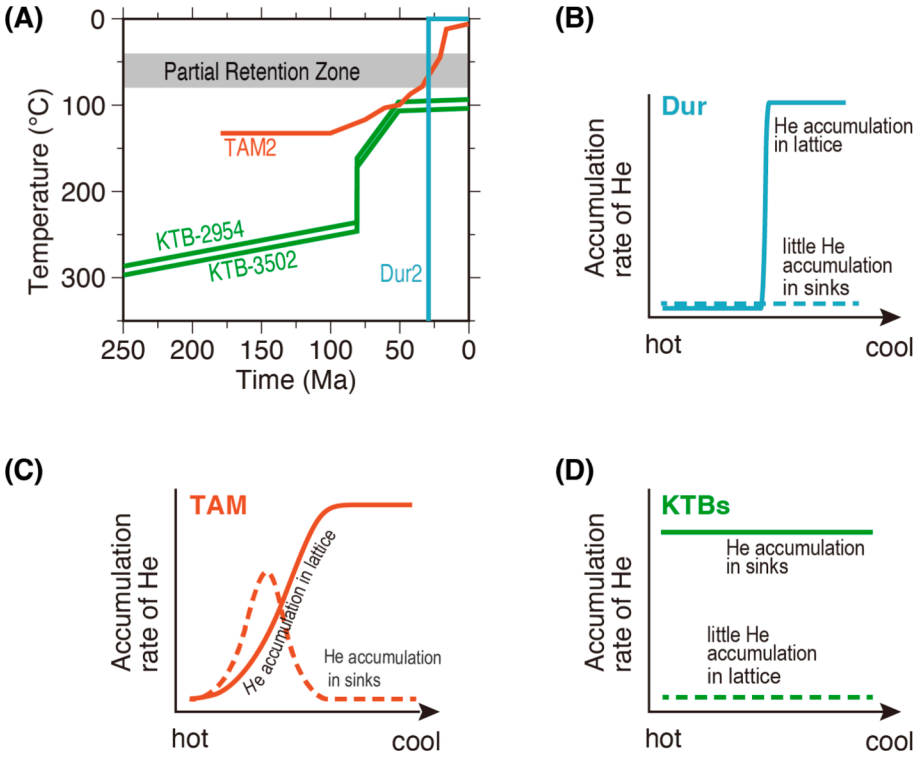

Fig. 7. **(A)** time–temperature paths of the analyzed samples. **(B)**, **(C)**, and **(D)** conceptual model of the accumulation of radiogenic ^{4}He in the crystal lattice through 'normal' volume diffusion and in diffusion sinks by including the trapping effect over geologic time, given the different thermal histories in **(A)**.

ideal candidate as its quenched thermal history and minimal sink abundance led to little geologic trapping. The KTB samples are also not ideal because they had low ^{4}He abundances and so greater uncertainties. In contrast, TAM2 yielded a clearly bimodal gas release, with robust signals that better define the grain's diffusion kinetics, making forward modeling more feasible. Additionally, this sample has no large gas spikes, avoiding complications related to this phenomenon.

In our modeling, our goal was not rigorous thermal-history inversion, as that is beyond the scope of the present study. Instead, our first-order objective was to reasonably simulate the observed gas release, including the proportion of gas released under the two peaks. Volume diffusion parameters were determined from ^{3}He observations. Because of the small trapping component of ^{3}He in TAM2 (i.e., ~ 20 % of total gas as high-temperature release, Fig. 3D), the effect of trapping on shifting the fractional loss and apparent diffusivities is minor (orange circles versus pale orange circles, Fig. 6C). We therefore directly used the apparent $\ln(D/a^2)$ to extract kinetics. Additionally, this approach is also beneficial for producing foreword modeled apparent kinetics that can be directly compared to the observations (Fig. 8C). Diffusion sinks with various abundances and sink escape activation energies were used to simulate laboratory ^{3}He release that is reasonably similar to our step-heating observation (orange points, Fig. 8A). These parameters are summarized in Table 2.

We find that the combined volume-diffusion and sink-trapping kinetics can simulate laboratory ^{4}He release that is close to the form and peak proportions of the dual-peak release observed in the step-heating experiment (green points, Fig. 8A) by using the thermal history adapted from AFT constraints (Fitzgerald et al., 2006) as inputs. The ratio evolution (Fig. 8B) and kinetics (Fig. 8C) are also comparable to our observations. Other alternative thermal histories, including monotonic

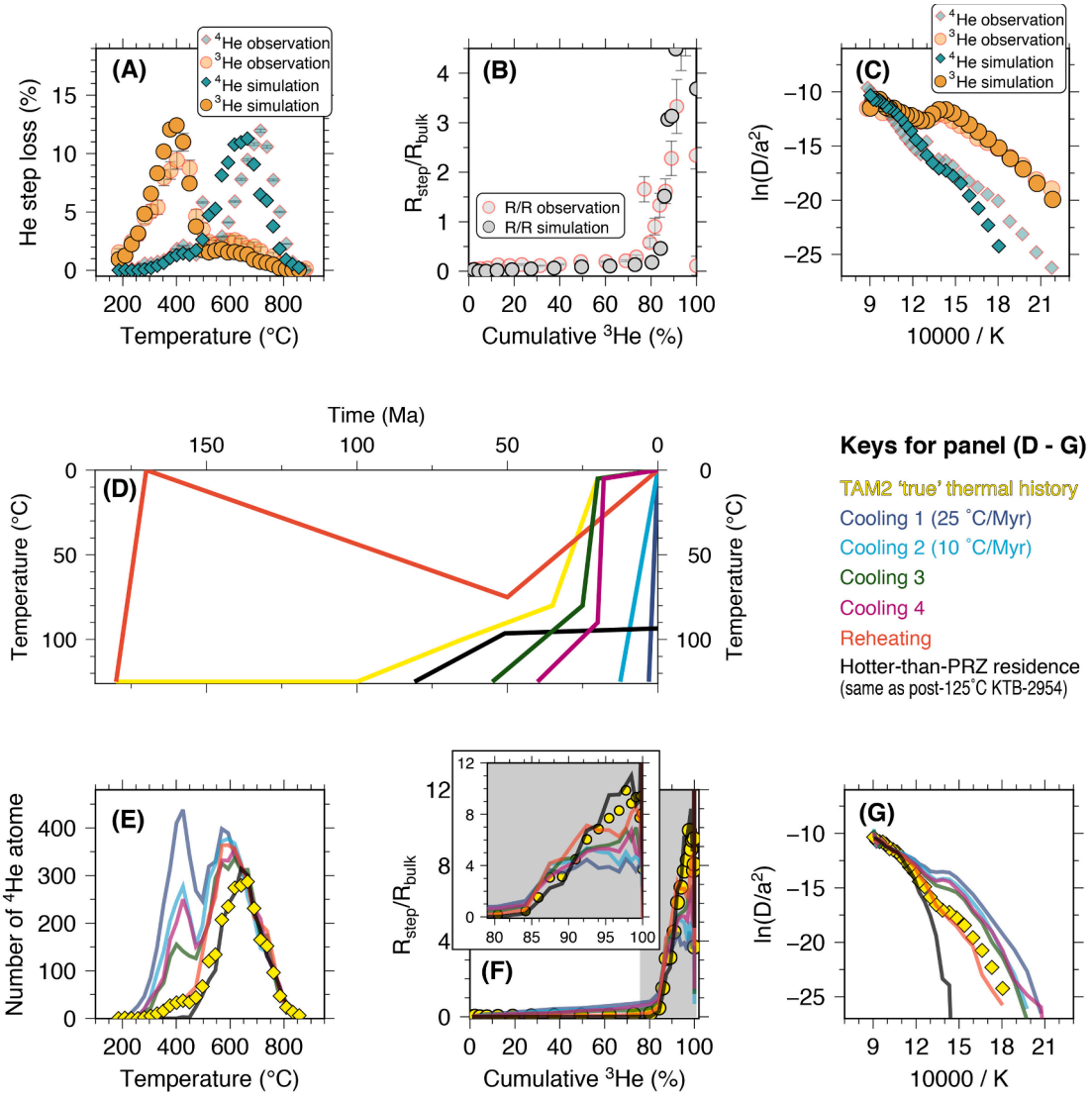

Fig. 8. DIFFSIM predictions of ^{3}He and ^{4}He releases **(A)** and the corresponding ratio evolution diagram **(B)** and Arrhenius data **(C)** for sample TAM2 compared to the laboratory ^{4}He and ^{3}He observations, assuming the TAM2 'true' geologic thermal history for ^{4}He. **(D)** Alternative thermal histories we used to predict ^{4}He releases using the same volume diffusion and sink kinetics, shown as the number of ^{4}He atoms degassed as a function of temperature **(E)** as well as the predicted ratio evolutions **(F)** and ^{4}He Arrhenius data **(G)**. Data points are simplified as connected lines in order to allow clarity in **(E)-(G)**. The inset in **(F)** illustrates part of the main plot that corresponds to 80–100% cumulative ^{3}He release in order to show detail.

Table 2
Modeling parameters used for simulation of helium diffusion and trapping in TAM2.

Volume Diffusion Parameters for TAM2			
Activation Energy		Diffusion Coefficient	Grain radius
21.4 Kcal/mol		2.97×10^{-3} cm^2/s	66 μm
Sink Trapping Parameters for TAM2			
Type #	Activation Energy	Temperature Scaling Factor	Number of Nodes as Sink
1	29 Kcal/mol	1200	250
2	32 Kcal/mol	1200	180
3	35 Kcal/mol	1200	150
4	38 Kcal/mol	1200	130
5	41 Kcal/mol	1200	100
6	44 Kcal/mol	1200	90
7	47 Kcal/mol	1200	30
8	51 Kcal/mol	1200	30
9	54 Kcal/mol	1200	30
10	57 Kcal/mol	1200	30

cooling paths with different cooling rates, reheating, and prolonged residence at temperature hotter than He PRZ (Fig. 8D) predict clearly distinguishable ^{4}He releases (Fig. 8E), ratio evolutions (Fig. 8F), and apparent kinetics (Fig. 8G).

Our forward modeling suggests that ^{4}He trapping in sinks should record time–temperature information, as evidenced by our successful reproduction of ^{4}He release using the ^{3}He-derived diffusion systematics and the known thermal-history information (Fig. 8A, B). Moreover, the ^{4}He release predicted for alternative thermal histories with the same sink characteristics are substantially different from the observed ^{4}He release. One caveat is that the sample TAM2 might represent an extreme case: the volume-diffusion parameters for the bulk crystal (i.e., non-sink parts) are considerably more diffusive than commonly cited kinetics for Durango apatite. This is an important, though counterintuitive, observation, because a more diffusive bulk crystal will allow more frequent helium random walking at the same temperature condition. Therefore, more radiogenic ^{4}He could migrate into sinks that would otherwise be lost if no sinks existed. Together, the combined diffusive lattice and retentive sink characteristics of this sample allow efficient gas retention that is evidenced by one of our model predictions made from the fastest monotonic cooling history (darker blue line, Fig. 8D, E). Even with a cooling rate of 25 °C/Ma, about half of the ^{4}He atoms are released under the high-temperature release peak (Fig. 8E). Such dominant high-temperature release appears to be rare given the study done by McDannell et al. (2018) and Guo et al. (2021). However, taken as a whole, our modeling results show promise that it might be possible to extract thermal history information from samples containing diffusion sinks.

4.5. *Implications for interpreting ^{4}He/^{3}He datasets with current helium diffusion models*

Our modeling of TAM2 suggests that, if we can characterize the kinetics associated with helium diffusion sinks from the proton-induced ^{3}He and incorporate these kinetics into our helium diffusion models, we can obtain more well-resolved thermal history information from sink-bearing samples. However, how well would current helium diffusion models (i.e., quantitative models that do not account for diffusion sink effects) do for sink-bearing samples?

It has become a common practice to use R_{step}/R_{bulk} data from ^{4}He/^{3}He thermochronometry to infer thermal history of samples (e.g., Shuster et al., 2005; Tremblay et al., 2015; Valla et al., 2012). In all published cases that we are aware of, the R_{step}/R_{bulk} data used to infer thermal history information either plot exclusively within the range of ^{4}He/^{3}He values permitted by volume diffusion models or have sample-specific information about parent nuclide zonation incorporated into these models. Many of the R_{step}/R_{bulk} data we present here cannot be used to infer thermal history information using existing models of helium diffusion in apatite (Flowers et al., 2009; Gautheron et al., 2009; Willett et al., 2017). Without accounting for diffusion sinks, these models would be unable to predict our observed R_{step}/R_{bulk} data for most geologic thermal histories. Moreover, in this study the observed ^{3}He data indicate that these complex R_{step}/R_{bulk} data cannot be explained solely by parent nuclide zonation, as parent nuclide zonation will not directly contribute to complex ^{3}He release behavior, which has been demonstrated by simulations of helium outgassing of grains with various kinds of parental zonation (McDannell et al., 2018). An important question then arises: if diffusion sinks are present in samples that exhibit less extreme R_{step}/R_{bulk} data, such that the observed ^{4}He/^{3}He ratios are within the range of values permissible via volume diffusion, will we recover accurate thermal history information if we do not include information about sink kinetics?

For sink-bearing apatite samples, characterizing the trapping behavior of ^{4}He might not always be necessary for the application of ^{4}He/^{3}He thermochronometry to some geologic problems. First, for 'quenched' apatite grains, the laboratory determined R_{step}/R_{bulk} data should remain useful whether or not diffusion sinks exist in the crystal, as evidenced by our Durango apatite experiments (sample Dur2, Fig. 2B), although this sample is special in that no alpha-ejection exists. Second, since many ^{4}He/^{3}He thermochronometry applications involve rapidly cooled samples (e.g., Shuster et al., 2005; Tremblay et al., 2015; Valla et al., 2012), we expect the geologic trapping of ^{4}He to be insignificant. Trapping will therefore largely stem from laboratory heating, having a similar impact on both radiogenic ^{4}He and proton-induced ^{3}He, and therefore not impact the ^{4}He/^{3}He evolution diagram. However, using laboratory determined R_{step}/R_{bulk} data for geologic thermal history extraction when the cooling rates are moderate or slow could prove challenging if diffusion sinks are present, as this could result in non-trivial geologic trapping. To demonstrate this, Fig. 9 presents ^{4}He/^{3}He ratio evolution diagrams created from DIFFSIM simulations of two end-member simple thermal histories involving monotonic cooling at rates of 100 °C/Ma (i.e., very fast cooling, Fig. 9A, C) and 20 °C/Ma (moderate cooling, Fig. 9B, D). For the DIFFSIM simulations, we assume that apatite has a typical Durango-like volume-diffusion (i.e., E_a of 33 Kcal/mol and D_0 of 50 cm^2/s; Farley, 2000) and sink characteristics as we used in the TAM2 simulations. The faster cooling simulation shows somewhat elevated R_{step}/R_{bulk} values for the > 80 % part of cumulative ^{3}He release, whereas the moderate cooling results in R_{step}/R_{bulk} data points well exceeding 1.6 for the latest heating steps. We then carried out forward model simulations of the ^{4}He/^{3}He spectra for 1500 randomly generated thermal histories following the approach of Schildgen et al. (2010). These forward models use the RDAAM kinetic model (Flowers et al., 2009), which essentially represents what most users with no sample-specific kinetics information would do when inferring thermal history information from ^{4}He/^{3}He data. We found that the faster cooling history (100 °C/Ma; Fig. 9A, B) can be well recovered by the RDAAM kinetics, but when the cooling rate is lower, the fits to synthetic data are less statistically robust (Fig. 9C, D). For the slower cooling scenario, none of the RDAAM-based models can predict the high R_{step}/R_{bulk} ratios at the end of the experiment, so the misfit with the observed ^{4}He/^{3}He spectrum is always poor. Because there is less trapping in the faster cooling scenario, the RDAAM-based model is still able to predict the observed ^{4}He/^{3}He spectrum that is characterized by the slightly elevated ^{4}He/^{3}He ratios at the end of the experiment reasonably well. As most ^{4}He/^{3}He datasets are collected without the precise temperature control necessary to recover sample-specific diffusion kinetics, some strategies for interpreting ^{4}He/^{3}He datasets can be implemented that facilitate the identification of samples impacted by diffusion sinks. For example, as linear heating ramps like the heating schedules we utilize in this work are not efficient for routine ^{4}He/^{3}He analysis, heating experiments can be designed with prograde heating steps that

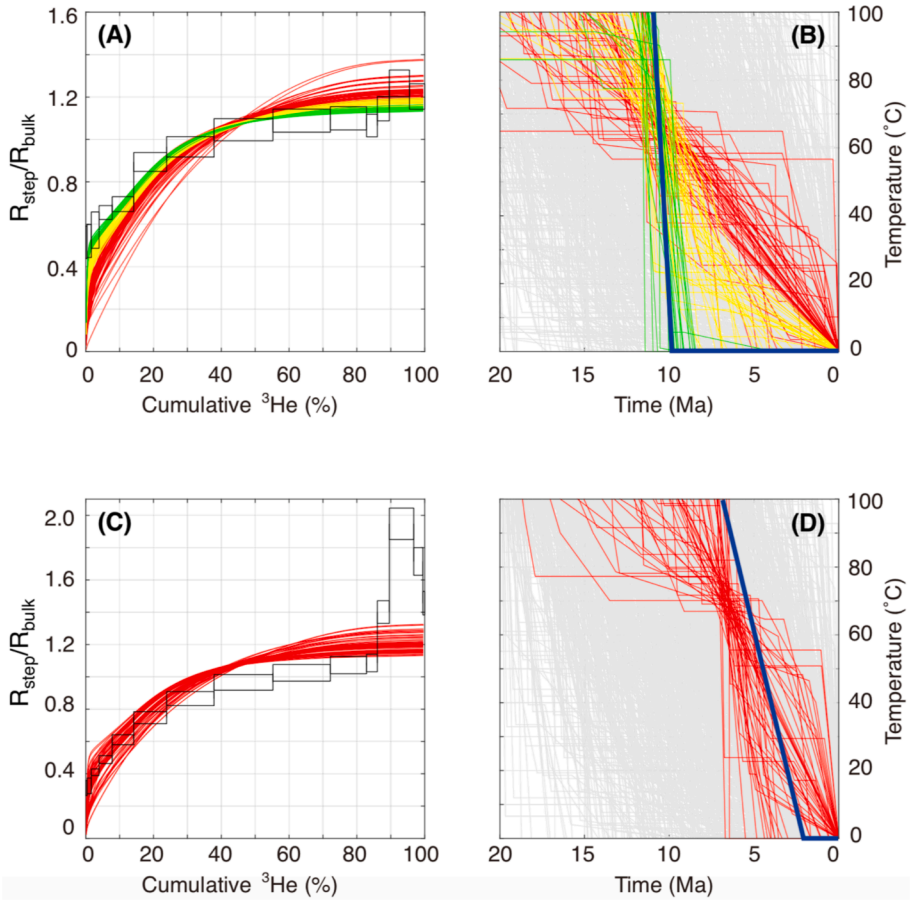

Fig. 9. (A) Synthetic ratio evolution diagram generated with DIFFSIM as a representation for a plausible ^{4}He/^{3}He spectrum from a sink-bearing sample. 1σ uncertainties are estimated at 5 % for each synthetic heating step, except for the first three and last five steps for which the uncertainties are set to 15 %, reflecting the fact that those steps often release less than 2 % of total gas and therefore often have larger analytical uncertainties during laboratory heating. Color curves are a set of inversions from 1500 random time–temperature (t-T) paths shown in (B) that predict the synthetic (U-Th)/He age generated by DIFFSIM. The thick line indicates the thermal history used for generating the synthetic data. Grey lines: all t-T paths. Red, yellow, and green lines in (B) and curves in (A) are based on the misfit between the predicted and synthetic ^{4}He/^{3}He spectrum using misfit statistic values of $\geq$ 4, 2–4, and $<$ 2, respectively, as defined by Schildgen et al. (2010). The lower two panels (C-D) illustrate similar inversion experiment but using a different t-T input with a more moderate cooling rate to generate the synthetic data in DIFFSIM.

involve enough high temperature steps before termination of heating to ensure detection of potential sink-related trapping. When examining ^{4}He/^{3}He datasets, one can also screen for and exclude sample aliquots that have too-low R_{step}/R_{bulk} ratios at the beginning of the experiment and/or too-high R_{step}/R_{bulk} ratios at the end of the experiment as being significantly impacted by diffusion sinks.

4.6. *Crystal imperfections and helium behavior*

Our work focuses on the systematics of helium mobilization in apatite samples that are affected by diffusion sinks, resulting in multimodal, complex helium release patterns associated with helium trapping (Figs. 2, 3, 4). The physical nature of sinks as described in this study is not understood but is most likely linked to certain types of crystal imperfections and requires further research. One such effort is the observation that dislocations from experimentally deformed Durango apatite appear to act as sinks (Guo et al., 2024b), yielding multimodal release peaks and complex ^{4}He/^{3}He spectra comparable to what we observe here. Voids, point defects (Gerin et al., 2017), and inclusions remain possible candidates for diffusion sinks as well that need to be studied. We posit that radiation damage likely does not behave as a sink, at least according to our current understanding of how radiation damage influences helium diffusion (Flowers et al., 2009; Gautheron et al., 2009; Willett et al., 2017). This is because all apatite contains some amount of radiation damage, however not all apatite samples exhibit trapping behavior like that seen in the ^{4}He/^{3}He experiments presented here or in CRH measurements (Guo et al., 2021, 2024a; McDannell et al., 2018). Further, the sinks seem to be largely thermally stable as suggested by the cycled heating perform by Guo et al. (2024a). In addition, we note that the crystal imperfections influencing helium diffusion kinetics are likely not limited to sinks. The well-known effects of radiation damage are in this category, but we posit that there are other types of non-sink imperfections that influence helium diffusivity too. This idea is supported by several observations. First, AHe ages from grains that exhibit a unimodal CRH pattern of ^{4}He release have shown dispersion significantly beyond what radiation damage models, such as RDAAM, predict (Guo et al., 2021, 2024a). Second, apparent diffusivities of ^{4}He vary significantly between intra-sample apatite grains that show unimodal ^{4}He release (Guo et al., 2021). This is further demonstrated by the volume diffusion kinetics parameters obtained from ^{3}He measurements in this study (e.g., the low activation energy of the low-temperature Arrhenius data for TAM2). In summary, crystal imperfections influence helium diffusion kinetics and behavior in apatite, but linking certain types of imperfections to changes in diffusivity or trapping behavior remains an open question that needs to be explored in future research.

5. Implications for other thermochronometers

Many reports of overdispersed (U-Th)/He ages and complex helium

laboratory release have been centered on apatite owing to its wide usage (e.g., Brown et al., 2013; Fitzgerald et al., 2006; Recanati et al., 2021). All our findings, however, can potentially be transferred to other thermochronometric systemics like zircon and titanite (U-Th)/He thermochronology. Perhaps, the immediate next step should be similar efforts on the mineral zircon given that zircon also often yields overdispersed (U-Th)/He ages (Godard et al., 2009; Tian et al., 2013; Wang et al., 2012). However, zircon also suffers from more extreme parent nuclide zonation, and the effects of radiation damage on helium diffusion are different in zircon than in apatite (Ginster et al., 2019; Guenthner et al., 2013). Complex ^{4}He laboratory release has been observed from pilot CRH analyses of zircon, exhibiting less systematic patterns as compared to ^{4}He release behavior from apatite grains (Idleman and Zeitler, 2021). It would be valuable to evaluate whether sink-related trapping, if it exists in zircon, is significant or not relative to factors like zonation and radiation damage in explaining this complex ^{4}He release. Zircon ^{4}He/^{3}He analysis is more likely to provide additional information to test if similar or different effects from diffusion sinks discussed in this work could be applied to the zircon (U-Th)/He system. While the titanite (U-Th)/He system is less developed than the apatite and zircon (U-Th)/He systems, dispersion of titanite (U-Th)/He ages and a similar negative correlation of age with eU has been observed (Baughman et al., 2017; Guenthner et al., 2017). In addition, studies on helium diffusion kinetics have been limited (Baughman et al., 2017; Cherniak and Watson, 2011; Reiners and Farley, 1999). These observations make titanite another mineral worth conducting experimental analysis on like in this work or using the CRH method.

On another related front, the apatite grains that exhibit complex helium diffusion in our step-heating experiments show Arrhenius arrays that are analogous to what argon diffusion in minerals like feldspar looks like that has been explained by the multiple diffusion domain (MDD) model (Harrison and Lovera, 2014; Lovera et al., 1989, 2002). There are both similarities and differences between MDD-like behavior for argon in feldspars and the results we present here. The two systems are similar in that as laboratory heating progresses, the diffusivities of helium or argon shift from arrays with higher apparent diffusivities to more retentive array(s). However, the models we present here to simulate helium behavior in apatite are different from MDD models, which do not allow the interaction of noble gas between different diffusion domains. Instead, in MDD models each domain functions independently of the other domains, and the frequently observed multiple Arrhenius arrays are interpreted to result from gas release from domains with different diffusion length scales. In contrast, we have modeled helium in apatite with a reversible trapping process in diffusion sinks inside a single volume diffusion domain. In this model, we are interpreting the shifts in Arrhenius array that we observe as being dictated by the varying kinetics of diffusion sinks. However, at this time the nature of crystal features and/or imperfections that result in MDD versus sink-trapping behavior are not understood. A clear understanding of the physical mechanisms driving complex noble gas diffusion behavior requires studies that directly target noble gas-crystal imperfection interactions (e.g., Guo et al., 2024b; Watson and Cherniak, 2003).

6. Conclusions

We carried out ^{4}He/^{3}He diffusion experiments on a suite of apatite samples that, based on previous studies, can exhibit complex release behavior of radiogenic ^{4}He, with the objective of better understanding the nature of this complex ^{4}He behavior by comparison with the concurrent release of proton-induced ^{3}He. Our work supports the hypothesis that diffusion sinks exist in apatite that impact the retention of radiogenic ^{4}He over geologic timescales, with the magnitude of the impact controlled in part by a sample's thermal history (Guo et al., 2024a; Zeitler et al., 2021). For the first time, trapping of ^{3}He is documented, and this confirms that diffusion sinks can trap helium in a laboratory-only process. The combined experimental data and forward simulations suggest that diffusion sinks could have different characteristics such as abundance and trapping kinetics that vary from grain to grain. Our forward modeling demonstrates the potential of describing diffusion and sink-trapping kinetics of helium in sink-bearing apatite via laboratory ^{3}He release data. Such kinetics information, along with a sample's known thermal history, is able to simulate the observed ^{4}He release, suggesting that thermal-history information can be extracted from sink-bearing apatite grains, provided that an inversion approach can be developed. Finally, the findings from this work may have implications for other accessory minerals used for thermochronometry, particularly zircon and titanite (U-Th)/He.

CRediT authorship contribution statement

Hongcheng Guo: Writing – review & editing, Writing – original draft, Visualization, Methodology, Investigation, Formal analysis, Data curation, Conceptualization. **Marissa M. Tremblay:** Writing – review & editing, Supervision, Resources, Methodology, Funding acquisition, Conceptualization. **Peter K. Zeitler:** Writing – review & editing, Software, Methodology, Funding acquisition, Conceptualization. **Bruce D. Idleman:** Writing – review & editing, Funding acquisition, Conceptualization. **Annia K. Fayon:** Writing – review & editing, Funding acquisition, Conceptualization.

Data availability

Data are available through Zenodo at https://doi.org/10.5281/zenodo.14714732.

Declaration of competing interest

The authors declare that they have no known competing financial interests or personal relationships that could have appeared to influence the work reported in this paper.

Acknowledgement

This research was supported by a Sloan Research Fellowship in Earth System Science, awarded to MMT by the Alfred P. Sloan Foundation (FG-2022-18729) and a National Science Foundation (NSF) grant to AKF (EAR-1727203) as well as PKZ and BDI (EAR-1726350). The TAM samples were originally collected as part of Antarctic fieldwork through the Antarctic Research Centre of Victoria University of Wellington with samples originally processed by Paul Fitzgerald at the University of Melbourne, Australia. KTB apatites were donations from Gunther Wagner and David Coyle. We thank W. Guenthner for carrying out U-Th-Sm measurements at the Helium Analysis Lab, University of Illinois Urbana-Champaign, which is supported by NSF grant EAR-1735788. We thank Kalin McDannell and John He for their thoughtful review comments. We thank Cécile Gautheron for both her additional review comments and editorial handling.

Appendix A. Supplementary material

Figure of step-heating results for KTB samples that yield exclusively simple degassing patterns, and figures of additional forward DIFFSIM models.

Supplementary material to this article can be found online at https://doi.org/10.1016/j.gca.2025.05.036.

References

Baughman, J.S., Flowers, R.M., Metcalf, J.R., Dhansay, T., 2017. Influence of radiation damage on titanite He diffusion kinetics. Geochim. Cosmochim. Acta 205, 50–64.

Beucher, R., Brown, R.W., Roper, S., Stuart, F., Persano, C., 2013. Natural age dispersion arising from the analysis of broken crystals: Part II. Practical application to apatite (U–Th)/He thermochronometry. Geochim. Cosmochim. Acta 120, 395–416.

Boyce, J.W., Hodges, K.V., 2005. U and Th zoning in Cerro de Mercado (Durango, Mexico) fluorapatite: insights regarding the impact of recoil redistribution of radiogenic 4He on (U–Th)/He thermochronology. Chem. Geol. 219, 261–274.
Brown, R.W., Beucher, R., Roper, S., Persano, C., Stuart, F., Fitzgerald, P., 2013. Natural age dispersion arising from the analysis of broken crystals. Part I: theoretical basis and implications for the apatite (U–Th)/He thermochronometer. Geochim. Cosmochim. Acta 122, 478–497.
Burnard, P.G., Farley, K.A., 2000. Calibration of pressure-dependent sensitivity and discrimination in Nier-type noble gas ion sources. Geochem. Geophys. Geosyst. 1, 7.
Cherniak, D.J., Watson, E.B., 2011. Helium diffusion in rutile and titanite, and consideration of the origin and implications of diffusional anisotropy. Chem. Geol. 288, 149–161.
Cooperdock, E.H.G., Ketcham, R.A., Stockli, D.F., 2019. Resolving the effects of 2-D versus 3-D grain measurements on apatite (U–Th) / He age data and reproducibility. Geochronology 1, 17–41.
Djimbi, D.M., Gautheron, C., Roques, J., Tassan-Got, L., Gerin, C., Simoni, E., 2015. Impact of apatite chemical composition on (U-Th)/He thermochronometry: an atomistic point of view. Geochim. Cosmochim. Acta 167, 162–176.
Drake, H., Reiners, P.W., 2021. Thermochronologic perspectives on the deep-time evolution of the deep biosphere. Proc. Natl. Acad. Sci. 118, e2109609118.
Farley, K.A., 2000. Helium diffusion from apatite: general behavior as illustrated by Durango fluorapatite. J. Geophys. Res. 105, 2903–2914.
Farley, K.A., 2002. (U-Th)/He dating: techniques, calibrations, and applications. Rev. Mineral. Geochem. 47, 819–844.
Fechtig, H., Kalbitzer, S., 1966. The Diffusion of Argon in Potassium-Bearing Solids. In: Schaeffer, O.A., Zähringer, J. (Eds.), Potassium Argon Dating. Springer, Berlin Heidelberg, Berlin, Heidelberg, pp. 68–107.
Fitzgerald, P.G., Baldwin, S.L., Webb, L.E., O'Sullivan, P.B., 2006. Interpretation of (U–Th)/He single grain ages from slowly cooled crustal terranes: a case study from the Transantarctic Mountains of southern Victoria Land. Chem. Geol. 225, 91–120.
Flowers, R.M., Ketcham, R.A., Shuster, D.L., Farley, K.A., 2009. Apatite (U–Th)/He thermochronometry using a radiation damage accumulation and annealing model. Geochim. Cosmochim. Acta 73, 2347–2365.
Gautheron, C., Pinna-Jamme, R., Derycke, A., Ahadi, F., Sanchez, C., Haurine, F., Monvoisin, G., Barbosa, D., Delpech, G., Maltese, J., Sarda, P., Tassan-Got, L., 2021. Technical note: analytical protocols and performance for apatite and zircon (U–Th) / He analysis on quadrupole and magnetic sector mass spectrometer systems between 2007 and 2020. Geochronology 3, 351–370.
Gautheron, C., Tassan-Got, L., Barbarand, J., Pagel, M., 2009. Effect of alpha-damage annealing on apatite (U–Th)/He thermochronology. Chem. Geol. 266, 157–170.
Gautheron, C., Zeitler, P.K., 2020. Noble gases deliver cool dates from hot rocks. Elements 16, 303–309.
Gerin, C., Gautheron, C., Oliviero, E., Bachelet, C., Mbongo, D.D., Seydoux-Guillaume, A., Tassan-Got, L., Sarda, P., Roques, J., Garrido, F., 2017. Influence of vacancy damage on He diffusion in apatite, investigated at atomic to mineralogical scales. Geochim. Cosmochim. Acta 197, 87–103.
Ginster, U., Reiners, P.W., Nasdala, L., Chanmuang, N.C., 2019. Annealing kinetics of radiation damage in zircon. Geochim. Cosmochim. Acta 249, 225–246.
Godard, V., Pik, R., Lavé, J., Cattin, R., Tibari, B., de Sigoyer, J., Pubellier, M., Zhu, J., 2009. Late Cenozoic evolution of the central Longmen Shan, eastern Tibet: insight from (U-Th)/He thermochronometry. Tectonics 28.
Guenthner, W.R., Reiners, P.W., Chowdhury, U., 2016. Isotope dilution analysis of Ca and Zr in apatite and zircon (U-Th)/He chronometry. Geochem. Geophys. Geosyst. 17, 1623–1640.
Guenthner, W.R., Reiners, P.W., Drake, H., Tillberg, M., 2017. Zircon, titanite, and apatite (U-Th)/He ages and age-eU correlations from the Fennoscandian Shield, southern Sweden. Tectonics 36, 1254–1274.
Guenthner, W.R., Reiners, P.W., Ketcham, R.A., Nasdala, L., Giester, G., 2013. Helium diffusion in natural zircon: Radiation damage, anisotropy, and the interpretation of zircon (U-Th)/He thermochronology. Am. J. Sci. 313, 145–198.
Guo, H., Zeitler, P.K., Idleman, B.D., 2024a. Behavior of helium diffusion sinks in apatite: evidence from continuous ramped heating analysis of borehole and well-characterized samples. Earth Planet. Sci. Lett. 641, 118828.
Guo H., Fayon A. K., Tremblay M. M., Zeitler P. K. and Idleman B. D. (2024b) Investigating how deformation and pressure influence the behavior of helium in apatite. *2024 Goldschmidt Conference*.
Guo, H., Zeitler, P.K., Idleman, B.D., Fayon, A.K., Fitzgerald, P.G., McDannell, K.T., 2021. Helium diffusion systematics inferred from continuous ramped heating analysis of Transantarctic Mountains apatites showing age overdispersion. Geochim. Cosmochim. Acta 310, 113–130.
Harrison, T.M., Lovera, O.M., 2014. The multi-diffusion domain model: past, present and future. Geol. Soc. Lond. Spec. Publ. 378, 91–110.
Idleman B. D. and Zeitler P. K. (2021) Helium Release from Zircon: Insights from Continuous Ramped Heating Experiments. *17th International Conference on Thermochronology*.
Idleman, B.D., Zeitler, P.K., McDannell, K.T., 2018. Characterization of helium release from apatite by continuous ramped heating. Chem. Geol. 476, 223–232.
Ketcham R. A., Tremblay M., Abbey A., Baughman J., Cooperdock E., Jepson G., Murray K., Odlum M., Stanley J. and Thurston O. (2022) Report from the 17th International Conference on Thermochronology. *Authorea. April 11, 2022*.
Lovera, O.M., Grove, M., Harrison, T.M., 2002. Systematic analysis of K-feldspar $^{40}Ar/^{39}Ar$ step heating results II: relevance of laboratory argon diffusion properties to nature. Geochim. Cosmochim. Acta 66, 1237–1255.
Lovera, O.M., Richter, F.M., Harrison, T.M., 1989. The $^{40}Ar/^{39}Ar$ thermochronometry for slowly cooled samples having a distribution of diffusion domain sizes. J. Geophys. Res. 94, 17917–17935.
McDannell, K.T., Keller, C.B., Guenthner, W.R., Zeitler, P.K., Shuster, D.L., 2022. Thermochronologic constraints on the origin of the Great Unconformity. Proc. Natl. Acad. Sci. 119, e2118682119.
McDannell, K.T., Zeitler, P.K., Janes, D.G., Idleman, B.D., Fayon, A.K., 2018. Screening apatites for (U-Th)/He thermochronometry via continuous ramped heating: He age components and implications for age dispersion. Geochim. Cosmochim. Acta 223, 90–106.
McDowell, F.W., McIntosh, W.C., Farley, K.A., 2005. A precise $^{40}Ar–^{39}Ar$ reference age for the Durango apatite (U–Th)/He and fission-track dating standard. Chem. Geol. 214, 249–263.
Meesters, A.G.C.A., Dunai, T.J., 2002. Solving the production–diffusion equation for finite diffusion domains of various shapes: Part II. Application to cases with α-ejection and nonhomogeneous distribution of the source. Chem. Geol. 186, 347–363.
Min, K., Farley, K.A., Renne, P.R., Marti, K., 2003. Single grain (U–Th)/He ages from phosphates in Acapulco meteorite and implications for thermal history. Earth Planet. Sci. Lett. 209, 323–336.
Murray, K.E., Orme, D.A., Reiners, P.W., 2014. Effects of U–Th-rich grain boundary phases on apatite helium ages. Chem. Geol. 390, 135–151.
Recanati, A., Grozavu, N., Bennani, Y., Gautheron, C., Missenard, Y., 2021. Apatite (U-Th-Sm)/He date dispersion: first insights from machine learning algorithms. Earth Planet. Sci. Lett. 554, 116655.
Reiners, P.W., Ehlers, T.A., Zeitler, P.K., 2005. Past, present, and future of thermochronology. Rev. Mineral. Geochem. 58, 1–18.
Reiners, P.W., Farley, K.A., 1999. Helium diffusion and (U–Th)/He thermochronometry of titanite. Geochim. Cosmochim. Acta 63, 3845–3859.
Reiners, P.W., Farley, K.A., 2001. Influence of crystal size on apatite (U–Th)/He thermochronology: an example from the Bighorn Mountains. Wyoming. Earth Planet. Sci. Lett. 188, 413–420.
Schildgen, T.F., Balco, G., Shuster, D.L., 2010. Canyon incision and knickpoint propagation recorded by apatite 4He/3He thermochronometry. Earth Planet. Sci. Lett. 293, 377–387.
Shuster, D.L., Ehlers, T.A., Rusmoren, M.E., Farley, K.A., 2005. Rapid glacial erosion at 1.8 Ma revealed by $^{4}He/^{3}He$ thermochronometry. Science 310 (5754), 1668–1670.
Shuster, D.L., Farley, K.A., 2004. $^{4}He/^{3}He$ thermochronometry. Earth Planet. Sci. Lett. 217, 1–17.
Shuster, D.L., Farley, K.A., 2005. 4He/3He thermochronometry: theory, practice, and potential complications. Rev. Mineral. Geochem. 58, 181–203.
Shuster, D.L., Farley, K.A., 2009. The influence of artificial radiation damage and thermal annealing on helium diffusion kinetics in apatite. Geochim. Cosmochim. Acta 73, 183–196.
Shuster, D.L., Flowers, R.M., Farley, K.A., 2006. The influence of natural radiation damage on helium diffusion kinetics in apatite. Earth Planet. Sci. Lett. 249, 148–161.
Spiegel, C., Kohn, B., Belton, D., Berner, Z., Gleadow, A., 2009. Apatite (U–Th–Sm)/He thermochronology of rapidly cooled samples: the effect of He implantation. Earth Planet. Sci. Lett. 285, 105–114.
Tian, Y., Kohn, B.P., Gleadow, A.J.W., Hu, S., 2013. Constructing the Longmen Shan eastern Tibetan Plateau margin: insights from low-temperature thermochronology. Tectonics 32, 576–592.
Tremblay, M.M., Fox, M., Schmidt, J.L., Tripathy-Lang, A., Wielicki, M.M., Harrison, T. M., Zeitler, P.K., Shuster, D.L., 2015. Erosion in southern Tibet shut down at ~10 Ma due to enhanced rock uplift within the Himalaya. Proc. Natl. Acad. Sci. 112, 12030–12035.
Valla, P.G., van der Beek, P.A., Shuster, D.L., Braun, J., Herman, F., Tassan-Got, L., Gautheron, C., 2012. Late Neogene exhumation and relief development of the Aar and Aiguilles Rouges massifs (Swiss Alps) from low-temperature thermochronology modeling and 4He/3He thermochronometry. J. Geophys. Res. 117, F1.
Wang, E., Kirby, E., Furlong, K.P., van Soest, M., Xu, G., Shi, X., Kamp, P.J.J., Hodges, K. V., 2012. Two-phase growth of high topography in eastern Tibet during the Cenozoic. Nat. Geosci. 5, 640–645.
Warnock, A.C., Zeitler, P.K., Wolf, R.A., Bergman, S.C., 1997. An evaluation of low-temperature apatite UTh/He thermochronometry. Geochim. Cosmochim. Acta 61, 5371–5377.
Watson, E.B., Cherniak, D.J., 2003. Lattice diffusion of Ar in quartz, with constraints on Ar solubility and evidence of nanopores. Geochim. Cosmochim. Acta 67, 2043–2062.
Willett, C.D., Fox, M., Shuster, D.L., 2017. A helium-based model for the effects of radiation damage annealing on helium diffusion kinetics in apatite. Earth Planet. Sci. Lett. 477, 195–204.
Wolfe, M.R., Stockli, D.F., 2010. Zircon (U–Th)/He thermochronometry in the KTB drill hole, Germany, and its implications for bulk He diffusion kinetics in zircon. Earth Planet. Sci. Lett. 295 (1–2), 69–82.
Wolf, R.A., Farley, K.A., Silver, L.T., 1996. Helium diffusion and low-temperature thermochronometry of apatite. Geochim. Cosmochim. Acta 60, 4231–4240.
Young, E.J., Myers, A.T., Munson, E.L., 1969. FROM CERRO DE MERCADO, DURANGO, MEXICO. *Geological Survey Research 1969, Chapter D*.84.
Zeitler, P.K., Brown, R., Hackspacher, P., 2017a. Better tools for tracing the thermal history of rocks (Meeting report: Thermo2016: The 15th International Conference on Thermochronology; Maresias, Brazil, 18–23 September 2016). EOS 98.
Zeitler, P.K., Enkelmann, E., Thomas, J.B., Watson, E.B., Ancuta, L.D., Idleman, B.D., 2017b. Solubility and trapping of helium in apatite. Geochim. Cosmochim. Acta 209, 1–8.
Zeitler, P., Guo, H., Idleman, B., McDannell, K., 2021. He Diffusion Systematics in Apatite. ESS Open Archive.
Zeitler, P.K., Herczeg, A.L., McDougall, I., Honda, M., 1987. U-Th-He dating of apatite: a potential thermochronometer. Geochim. Cosmochim. Acta 51, 2865–2868.